Angewandte Chemie
Eine Zeitschrift der Gesellschaft Deutscher Chemiker

Supporting Information

Paper-Based Electrical Respiration Sensor

*Firat Güder, Alar Ainla, Julia Redston, Bobak Mosadegh, Ana Glavan, T. J. Martin, and George M. Whitesides**

anie_201511805_sm_miscellaneous_information.pdf

Sensor Characterization

We characterized the response of the sensors to RH in a system built in-house (Figure S0-1). It consisted of two mass-flow-controllers supplying dry and humidified N_2 streams. Both streams of nitrogen were controlled by a computer using LabView software. The electrical measurements were made with a Keithley 2400 source-meter. We designed the electrodes of the paper sensors to fit into the electrical connector in the measurement system such that eight sensors could be measured in parallel.

We purchased the procedure masks from CVS (CURAD Surgical Facemasks). This brand was chosen purely based on its widespread availability and low cost, but we anticipate that most other brands can also be used successfully.

Electronics and Software

We designed the reader electronics using off-the-shelf components purchased from Digikey (including the Arduino microcontroller). The printed circuit board (PCB) was designed using Eagle application package and was manufactured by Silver Circuits Sdb. Bhd., Selangot Malaysia. The Bluetooth shield, Kedsum KDF001A, for the Arduino board was purchased separately from Amazon. The housing for the electronics was designed using AutoCAD and printed with a Dimension; Stratasys, Inc 3D printer in acrylonitrile-butadiene-styrene (ABS) thermoplastic polymer.

We analysed the power characteristics of each subsystem as well as the entire device and the paper sensor (Figure S0-2). The system required a steady supply of 130 mA when all of the components, including the Bluetooth wireless link between the device and the tablet computer, were active at a 5V supply voltage. This corresponds to a power requirement of 650 mW. The power specifications can be substantially reduced through further optimization and redesign of the electrical circuit. The paper-sensor had the lowest power requirement among the electronic components used in the system with a peak power consumption of 500 µW (<0.05% of the entire system).

The Android app was designed and implemented in the Android Studio development environment using Java and XML programming languages. We used a Samsung Galaxy Tab 4 tablet computer for testing.

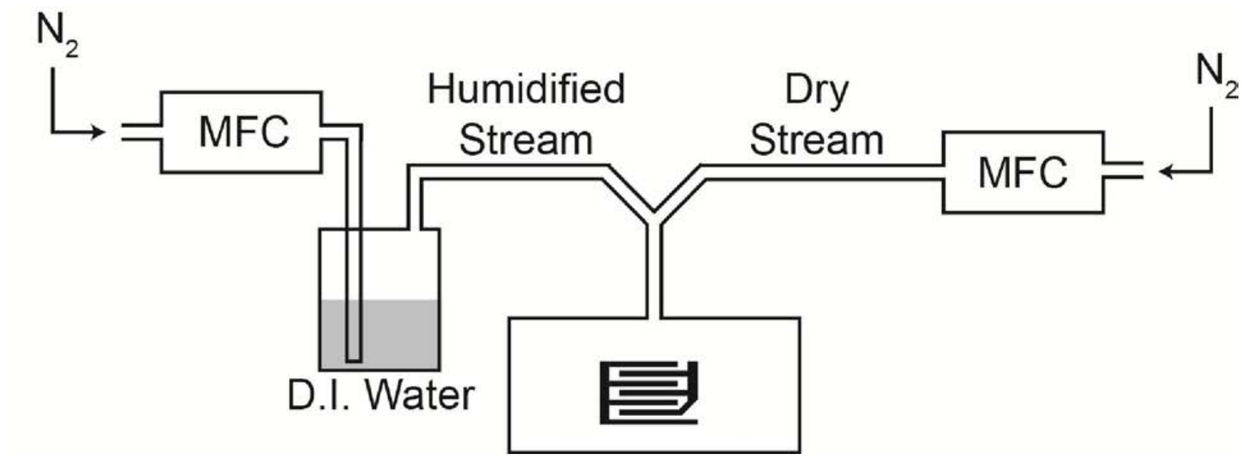

Figure S0-1. Schematic view of the system constructed to characterize the paper-based sensor. We used two mass flow controllers – MFC – to mix flows of humidified nitrogen and dry nitrogen to control the RH inside the measurement chamber. The humidified stream was created by bubbling nitrogen through a bottle containing deionized water (D.I. water)

Part	Voltage (V)	Current (mA)	Power (mW)	Percentage(%)
Battery (2x Li-ion cell). TOTAL	7.8	130	1014	100
Sensor (dry/min)	25	1.30E-03	0.0325	0.003
Sensor (humid/max)	25	2.00E-02	0.5	0.049
Bluetooth module	5	25	125	12
Amplifier board	5	36	180	18
Microcontroller board (Arduino)	3.3	69	227.7	22
Voltage conversion losses			481.3	47

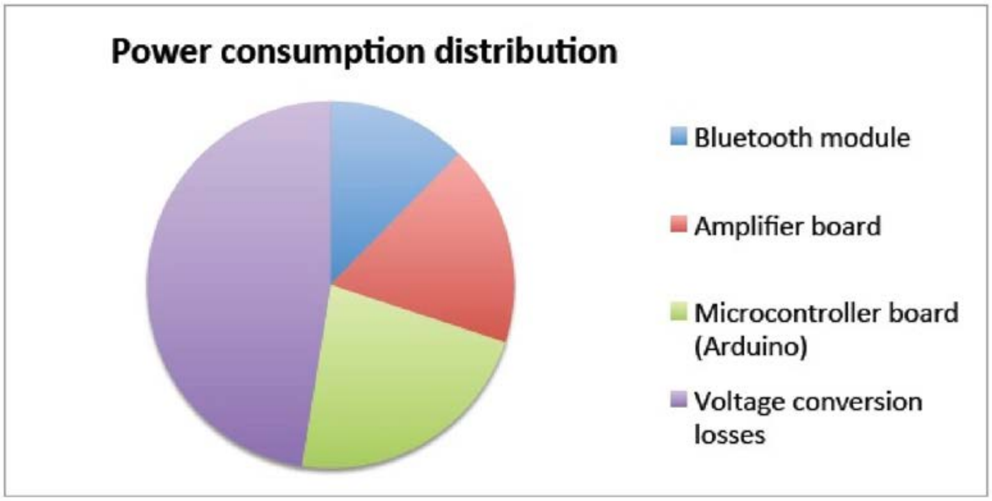

Figure S0-2. Power consumption distribution of the data acquisition electronics. The current design requires a steady supply of 130 mA. Our design has large voltage conversion losses and which can be eliminated by optimizing the system for power, especially the step-up DC-DC converter and voltage regulator circuitry. Reducing clock speed for the microcontroller board would also reduce power consumption

Electronic Design of the Amplifier Board

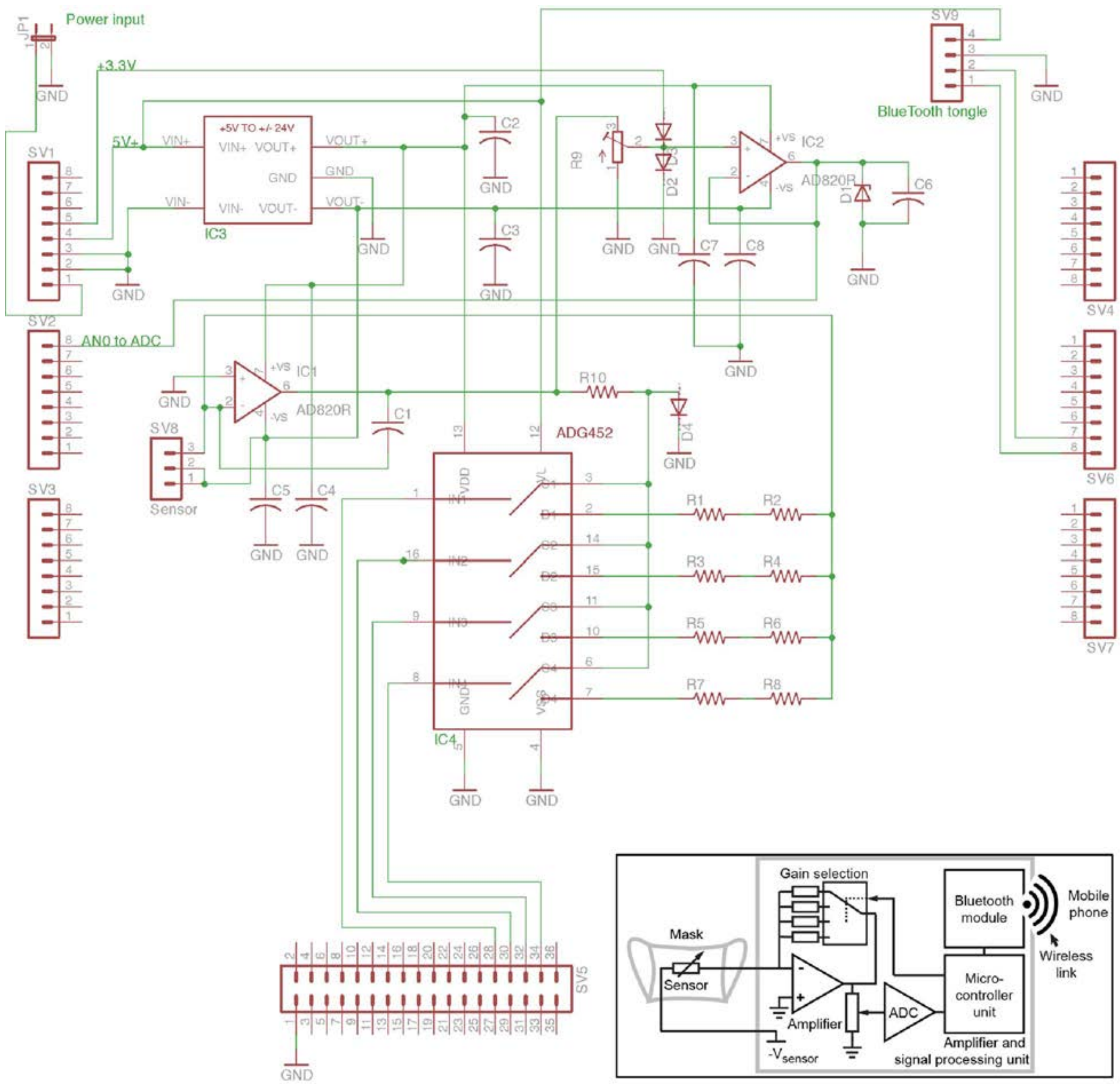

Figure S0-3. Detailed schematics of the design of amplifier board. The inset shows an overview of the entire system.

Symbol	Name/Value	Description
IC1	AD820ARZ-ND	Operational amplifier (op amp). Manufacturer: Analog Devices Inc.
IC2	AD820ARZ-ND	Operational amplifier (op amp). Manufacturer: Analog Devices Inc.
IC3	IA0524D	DC-DC converter +/-24V ouput from +5V input. Manufacturer: XP Power
IC4	ADG452BRZ-ND	Solid state analog switch (Quad, 4 switches in the same package). Manufacturer: Analog Devices Inc.
SV1,2,3,4, 6,7,8,9	Pin headers with 0.1inch step. One row	Pin headers SV1-7 connect the amplifier board to Arduino Due microcontroller board. Pin headers which are not used for electrical connections are still fixed for mechanical support. Pin header SV8 is connection to sensor and SV9 is connection to Bluetooth dongle. For connection map see table below.
SV5	Pin header with 0.1inch step. Two rows	Pin header SV is connecting the amplifier board to Arduino Due microcontroller board. For the connection map see table below.
D1	BZX84-C3V3	Zener diode 3.3V. Protects the Arduino analog input from signals with negative polarity or over voltage. Allowed input range is 0 to 3.3V
D2	LS4448GS08	Signal diode. Protects IC2 op amp input from negative polarity signals
D3	LS4448GS08	Signal diode. Protects IC2 op amp input from over 3.3V signals

D4	LS4448GS08	Signal diode. Protects the switch input from negative polarity signal.
R1,2	1MΩ	R1+R2=1Mohm. 1%, 0805 case. (Highest gain)
R3,4	10MΩ	R3+R4=10MOhm. 1%, 0805 case.
R5,6	20MΩ	R5+R6=20MOhm. 1%, 0805 case.
R7,8	50MΩ	R7+R8=50Mohm. 1%, 0805 case. (Lowest gain)
R9	100kΩ	Trimmer
R10	10kΩ	
C1	100pF	
C2	1μF	Op amp supply
C3	1μF	Op amp supply
C4	10nF	Rail stabilization of op amp
C5	10nF	Rail stabilization of op amp
C6	-	Not used in eventual design
C7	10nF	Rail stabilization of op amp
C8	10nF	Rail stabilization of op amp

Table S0-4. The part list with product code from Digi-Key (all parts were obtained from there)

Pinheader	Pin	External connection	Description
SV1	1	Arduino “Vin”	Arduino power input from battery (>+6-16V)
	2,3	Arduino “GND”	Ground
	4	Arduino “5V”	+5V from Arduino to amplifier board
	5	Arduino “3.3V”	+3.3V from Arduino to amplifier board
SV2	8	Arduino “A0”	Analog input 0

SV5	28	Arduino “D28”	Digital output 28. Gain selection. R_gain=R1+R2
	30	Arduino “D26”	Digital output 26. Gain selection. R_gain=R3+R4
	32	Arduino “D24”	Digital output 24. Gain selection. R_gain=R5+R6
	34	Arduino “D22”	Digital output 22. Gain selection. R_gain=R7+R8
SV6	7	Arduino “RX”	Connects the Bluetooth shield serial output to Arduino serial (USART) input
	8	Arduino “TX”	Connects the Bluetooth shield serial input to Arduino serial (USART) output
SV8	1,2	Sensor voltage	This provides the sensor voltage (-V approx. -25V)
	3	Sensor current input	This is kept on potential 0V and current is measured through this pin.
SV9	1	KDF001A RX	This connects the Bluetooth shield serial input to Arduino serial output
	2	KDF001A TX	This connects the Bluetooth shield serial output to Arduino serial input
	3	KDF001A ground	Ground connection to Bluetooth shield
	4	KDF001A power inp.	Power input to Bluetooth shield (+5V)

Table S0-5. Pinheaders map

Signal Processing Algorithm using Arduino Due Microcontroller Board

The microcontroller does the following:

Every 1ms collect one analog signal reading (ADC is 10-bit, giving values in the range 0 to 1023)

Integrate collected analog signal readings to reduce noise. Sum 25 readings.

If sum is less than 1500 (low reading), then try to increase the gain by multiplexing between different feedback resistors using Arduino digital outputs 22, 24, 26 or 28.

If sum is more than 14800 (high reading), then try to reduce the gain by multiplexing between different resistors using Arduino digital outputs 22, 24, 26 or 28.

Every 100ms send the reading over Bluetooth (write to Arduino UART output)

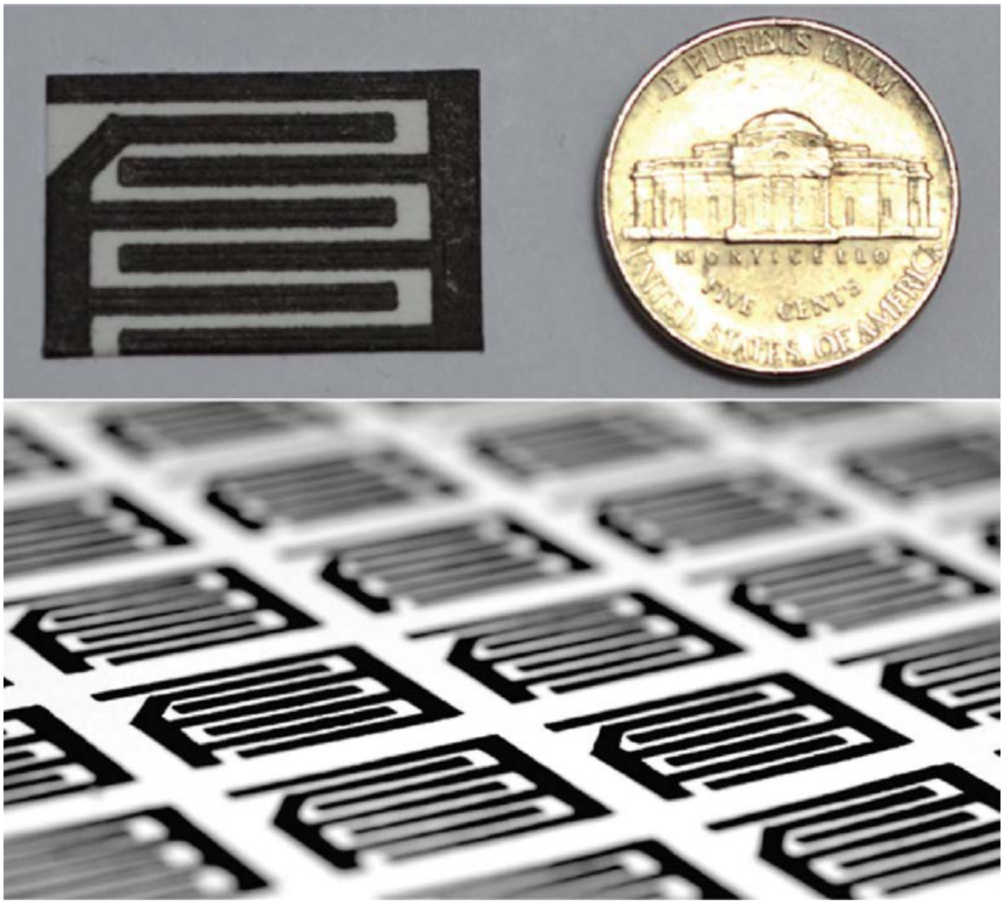

Figure S1. (Top) Paper-based printed respiration sensor next a US nickel (5 cents), **(Bottom)** Image of an array of sensors

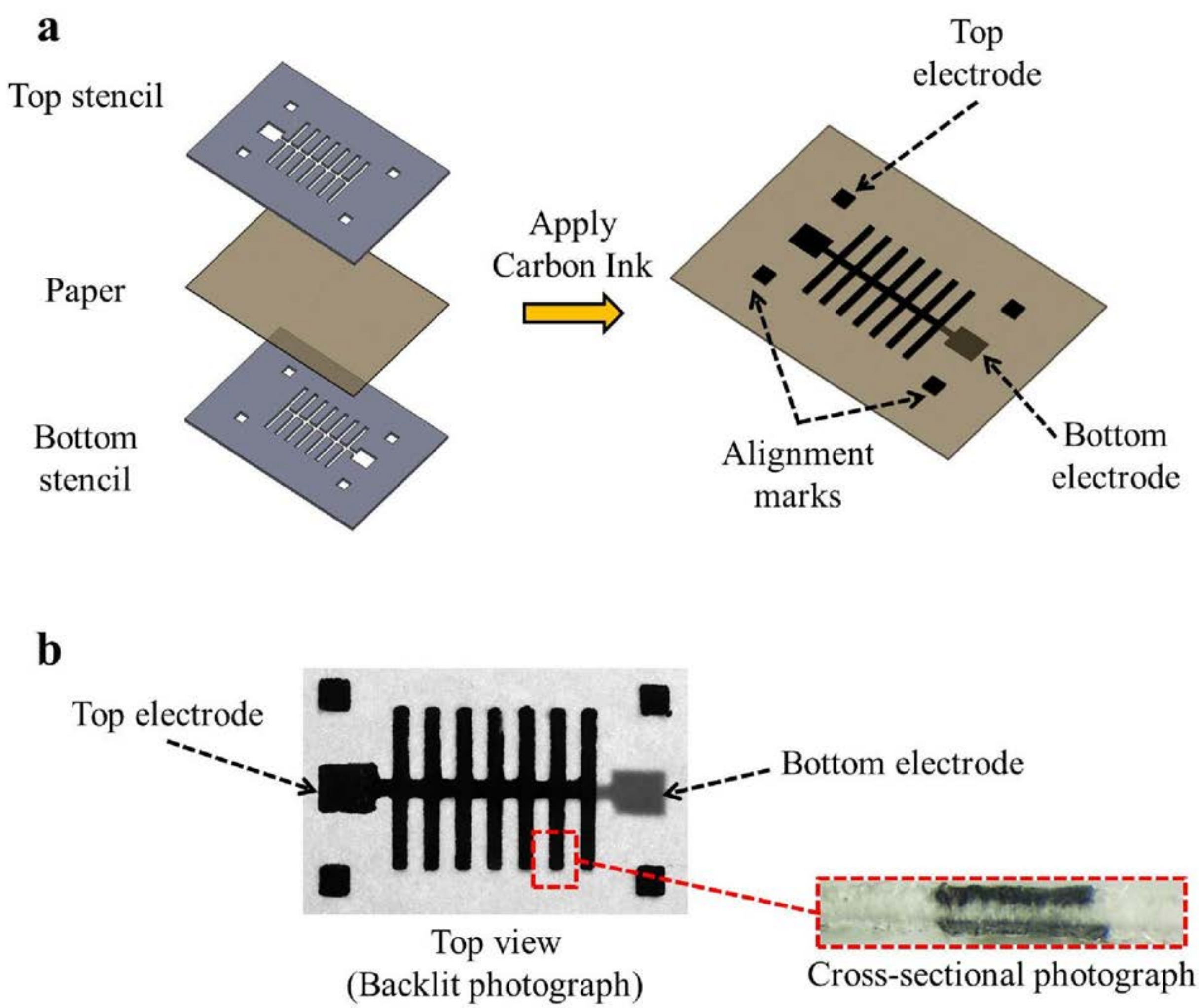

Figure S2. (A) Fabrication procedure of the paper sensor with aligned electrodes printed on both sides of paper (top and bottom) **(B)** Light photograph of an actual device. The light source is behind the device, showing the aligned electrodes at both the front and back of the paper.

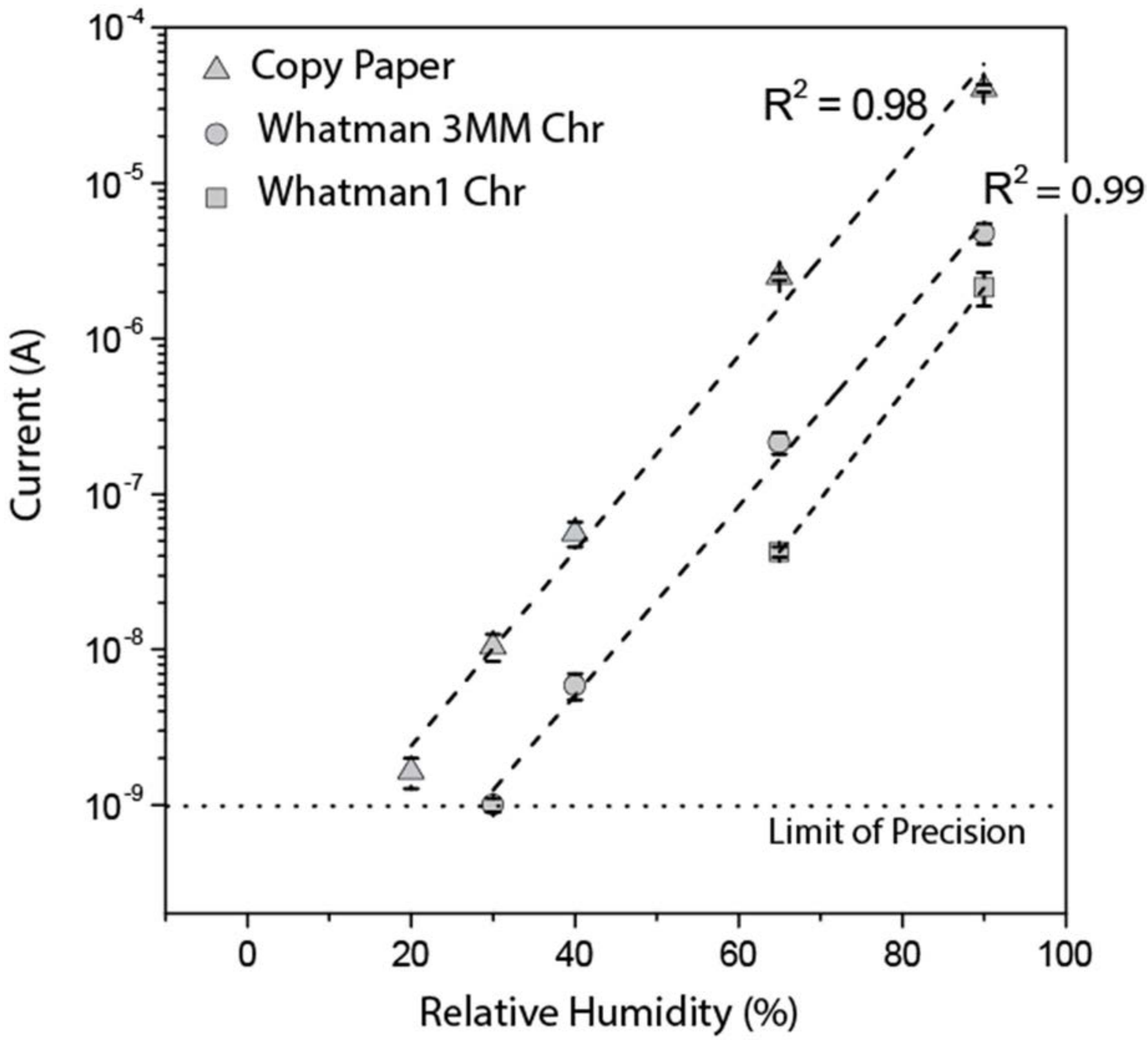

Figure S3. Electrical characterization of the paper-based moisture sensor, fabricated on different paper substrates. The error bars represent standard deviations (SD) for N = 7

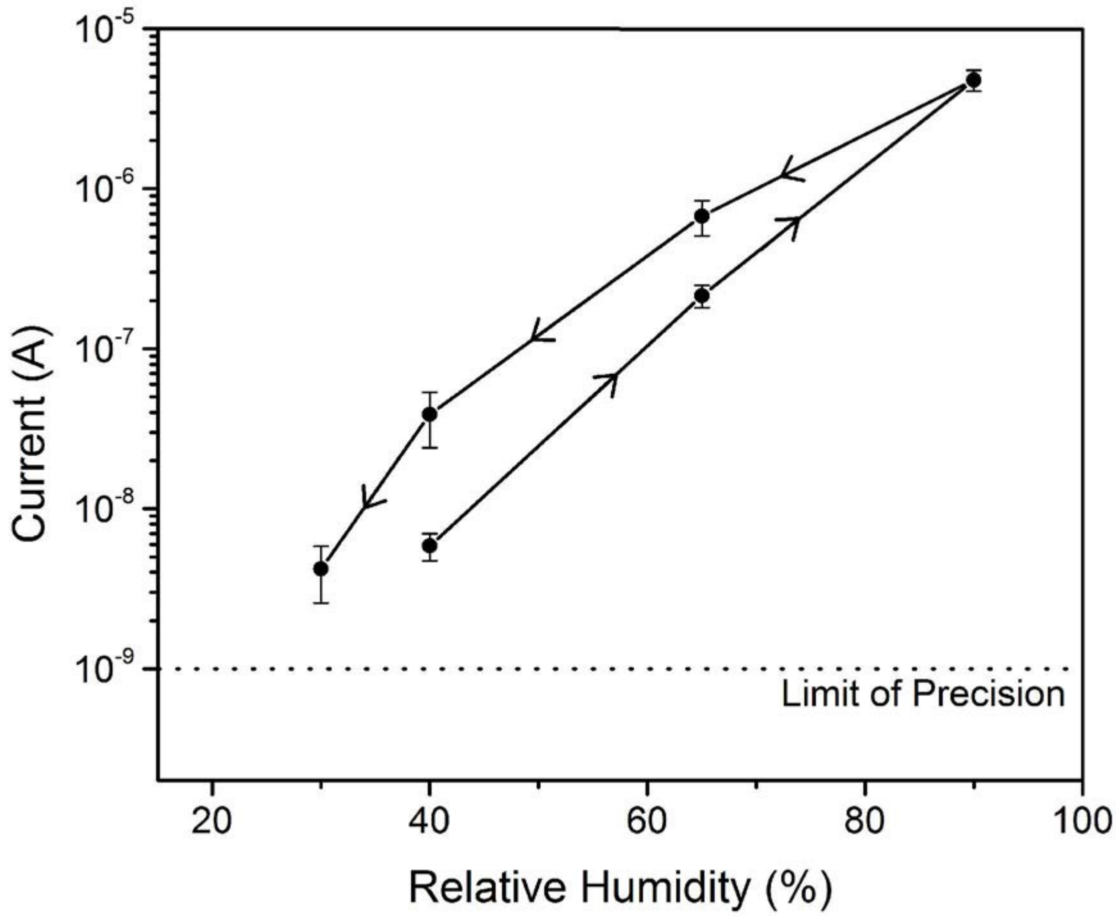

Figure S4. Hysteresis for the equilibrium output of the paper sensor. The chamber was set to 20%, 30%, 40%, 65% and 90% RH (increasing) and then decreased back to 20%. The paper sensor did not generate a detectable current below a RH of 30%, whether the RH was being increased or decreased. For each set point, the measurement was taken when the output signal reached a steady-state value (approximately an hour). Hysteresis in cellulose paper reflects the fact that the adsorption the desorption isotherms are different. [Roberts, J.C., 1996. "The chemistry of paper", Royal Society of Chemistry] Hysteresis is not a problem for our measurements, which are self-referenced, when the observed changes are transient, and when the system does not reach equilibrium (as for respiration).

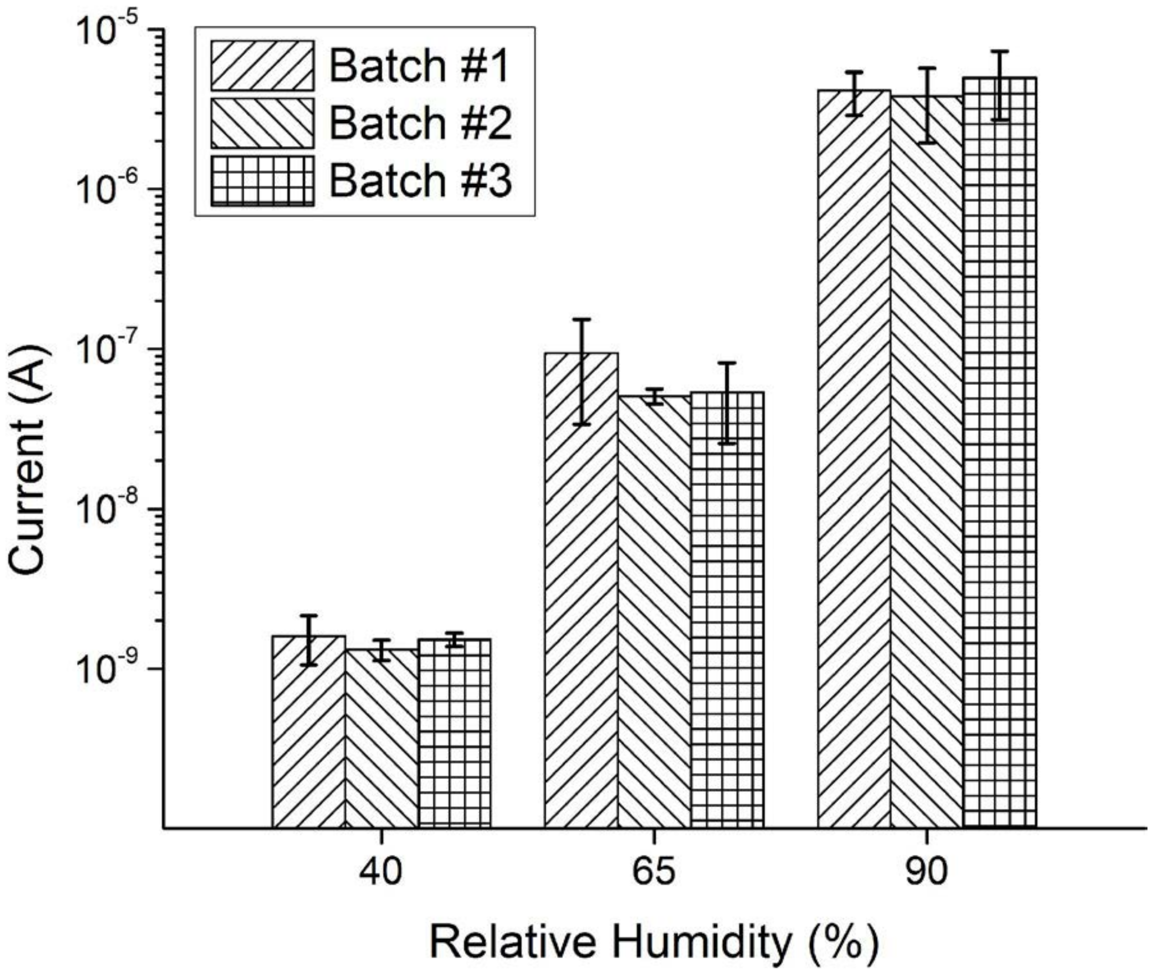

Figure S5. Batch-to-batch characterization of paper sensors at various levels of RH. The error bars indicate standard deviations (N=7).

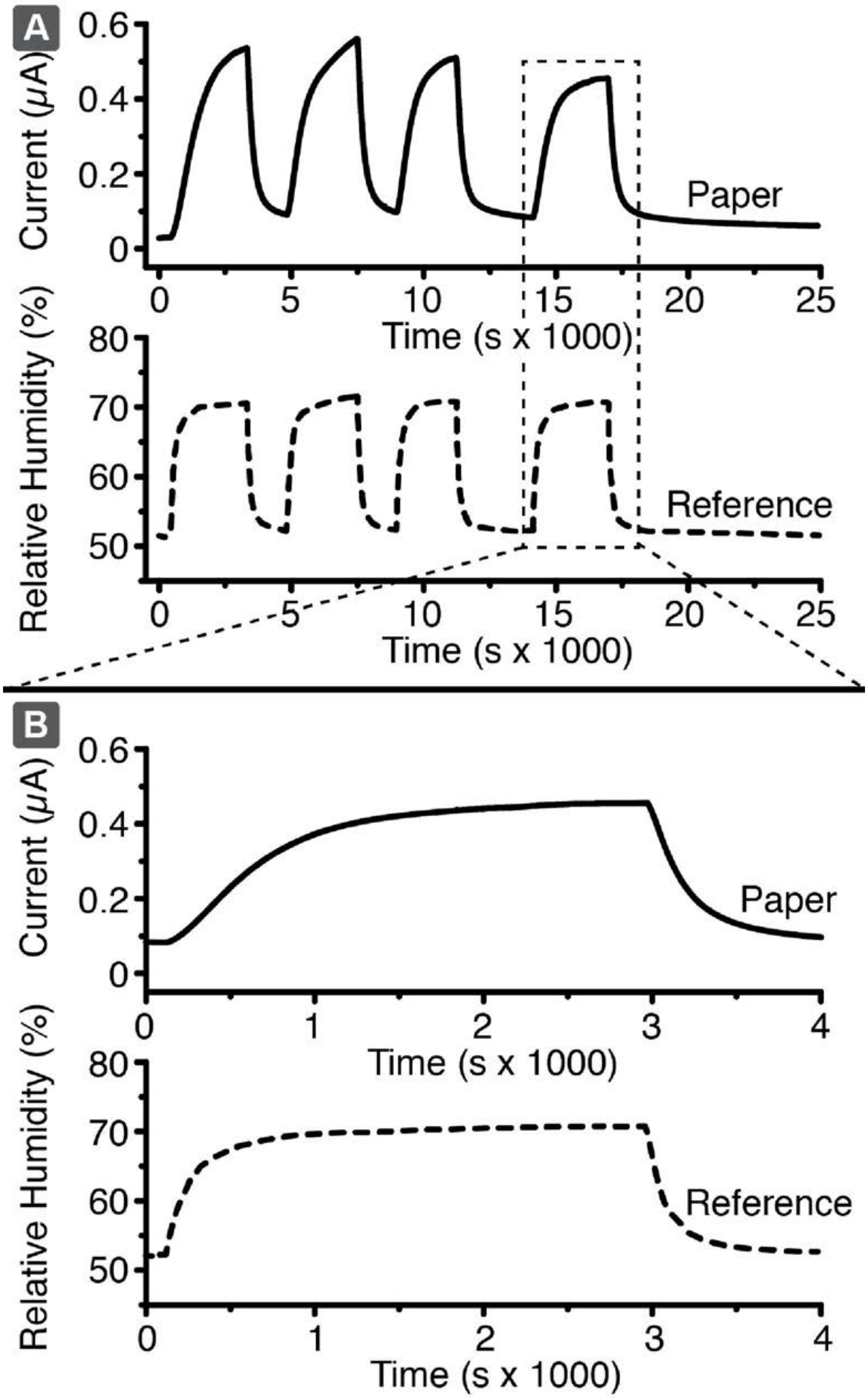

A
0.6
0.4
0.2
0
Current (μA)
Paper
0
5
10
15
20
25
Time (s x 1000)
80
70
60
50
Relative Humidity (%)
Reference
0
5
10
15
20
25
Time (s x 1000)
B
0.6
0.4
0.2
0
Current (μA)
Paper
0
1
2
3
4
Time (s x 1000)
80
70
60
50
Relative Humidity (%)
Reference
0
1
2
3
4
Time (s x 1000)

Figure S6. Response time of the paper sensor measured by changing the RH from 50% to 70% and back to 50%. This process was repeated four times. **(A)** The solid line (Paper) shows the response of the paper sensor, and the dashed line (Reference) is that of the reference sensor (a conventional Honeywell hih-4000 RH type sensor with a nominal response time of 15s). The chamber used to characterize the sensor reached the RH set point and equilibrated in ~600 sec (10 mins) in going from 50% RH to 70%. The paper sensor took ~1500 sec (25 mins) to reach steady-state **(B)**. When the RH inside the chamber was decreased from 70% to 50%, the transient response of the paper sensor was rapid (comparable to the $15 reference sensor).

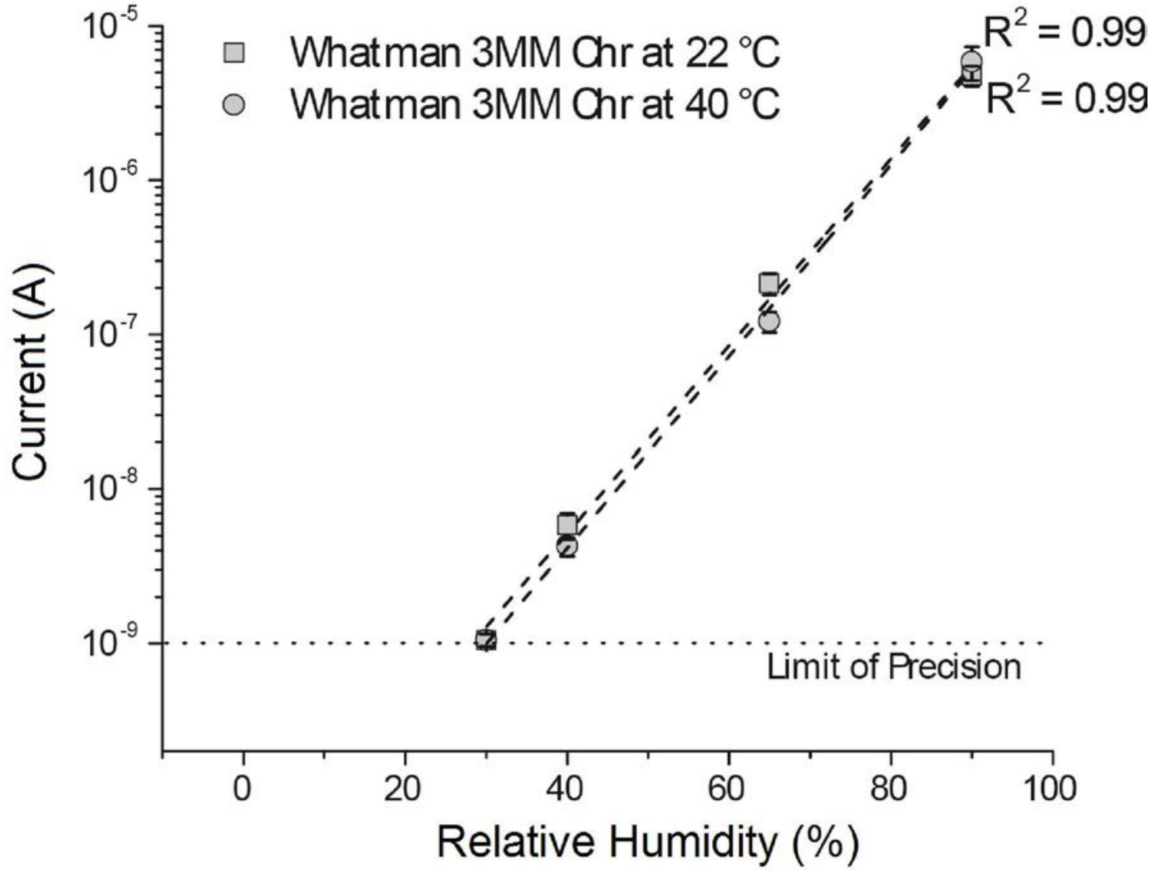

Figure S7. Characterization of paper-based moisture sensors at 22 ºC and 40 ºC. The error bars represent standard deviation (SD), N=7

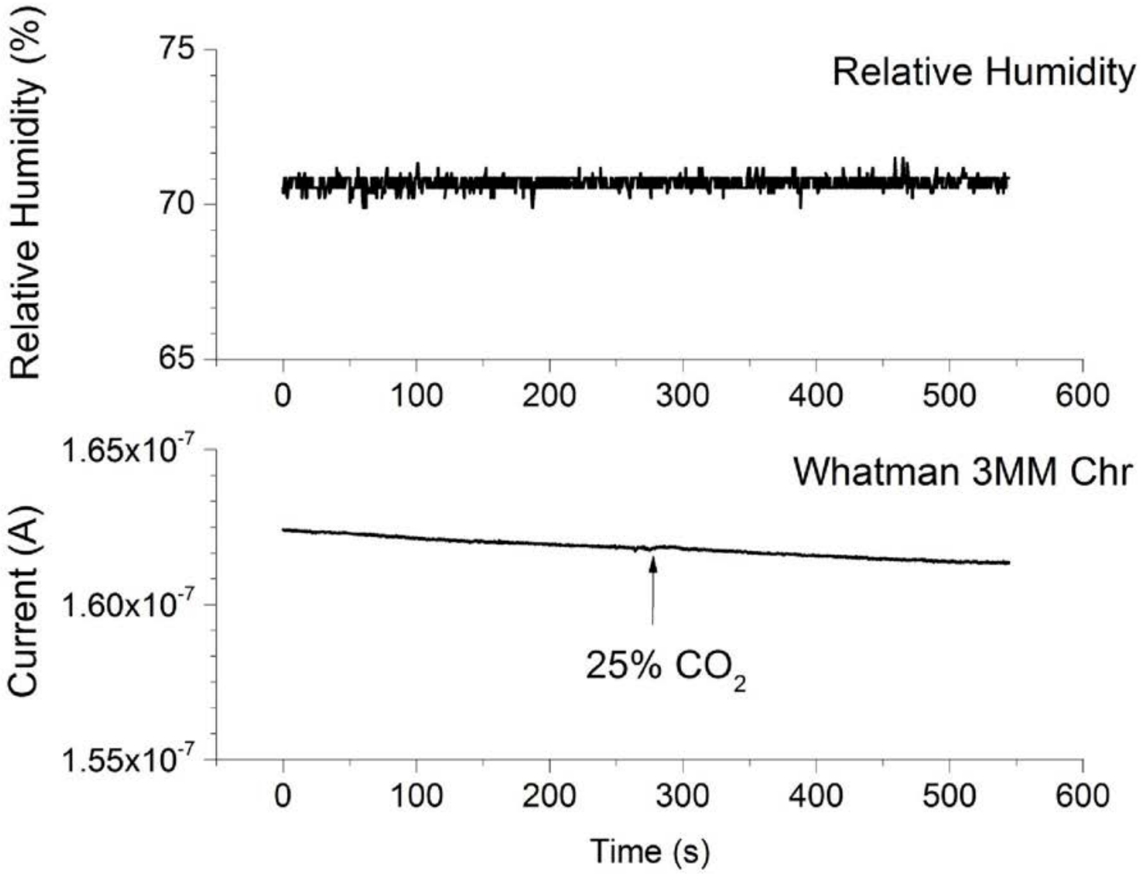

Figure S8. Response of the paper-based moisture sensor in the presence of CO_2. In this experiment, the dry N_2 stream is replaced with a CO_2 stream using a three-way T-valve at t = 270s as indicated by the arrow in the figure. There was no increase in the sensor output when the sensor was exposed to 25% v/v CO_2. The RH inside the test chamber was kept constant at approx. 70% during the experiment.

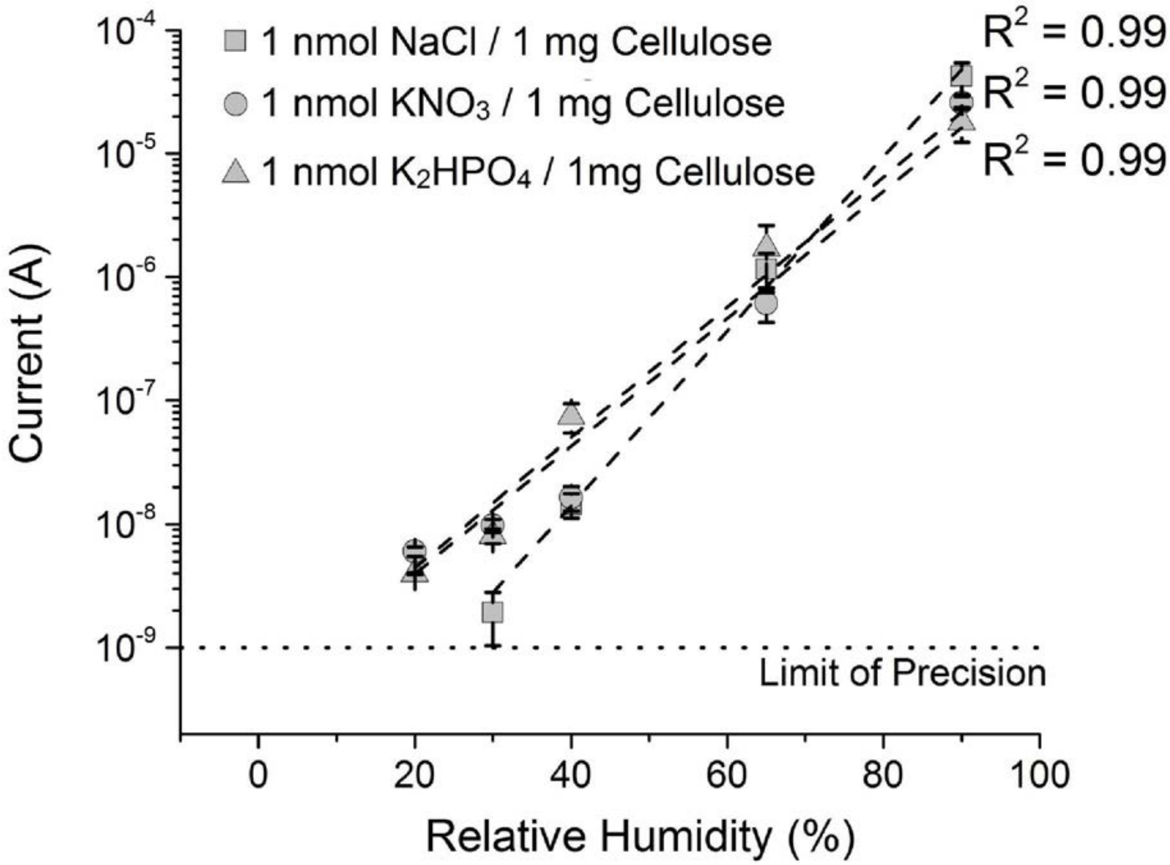

Figure S9. Characterization of paper-based moisture sensors with different salts (KNO_3, K_2HPO_4, NaCl) at the same concentration over a range of RH of 0-90%. We added 100 µL of 1mM (100 nmol) aqueous solution of KNO_3, K_2HPO_4, NaCl on a paper sensor fabricated using Whatman 3MM Chr paper and evaporated the excess water in a conventional oven at 60 ºC for one hour. To calculate the concentration of salt with respect to the amount of cellulose in paper, we cut a piece of Whatman 3MM Chr paper with the same size as the sensor (16 mm x 22 mm) without the electrodes and weighed it on an analytical balance (100 mg). The addition of 100 nmol of salt resulted in a concentration of 1 nmol of salt per 1 mg of cellulose. We presume, small differences in the signal level are due to variations in hygroscopicity of the salts and solubility of the salts in water. The error bars represent standard deviations (SD).

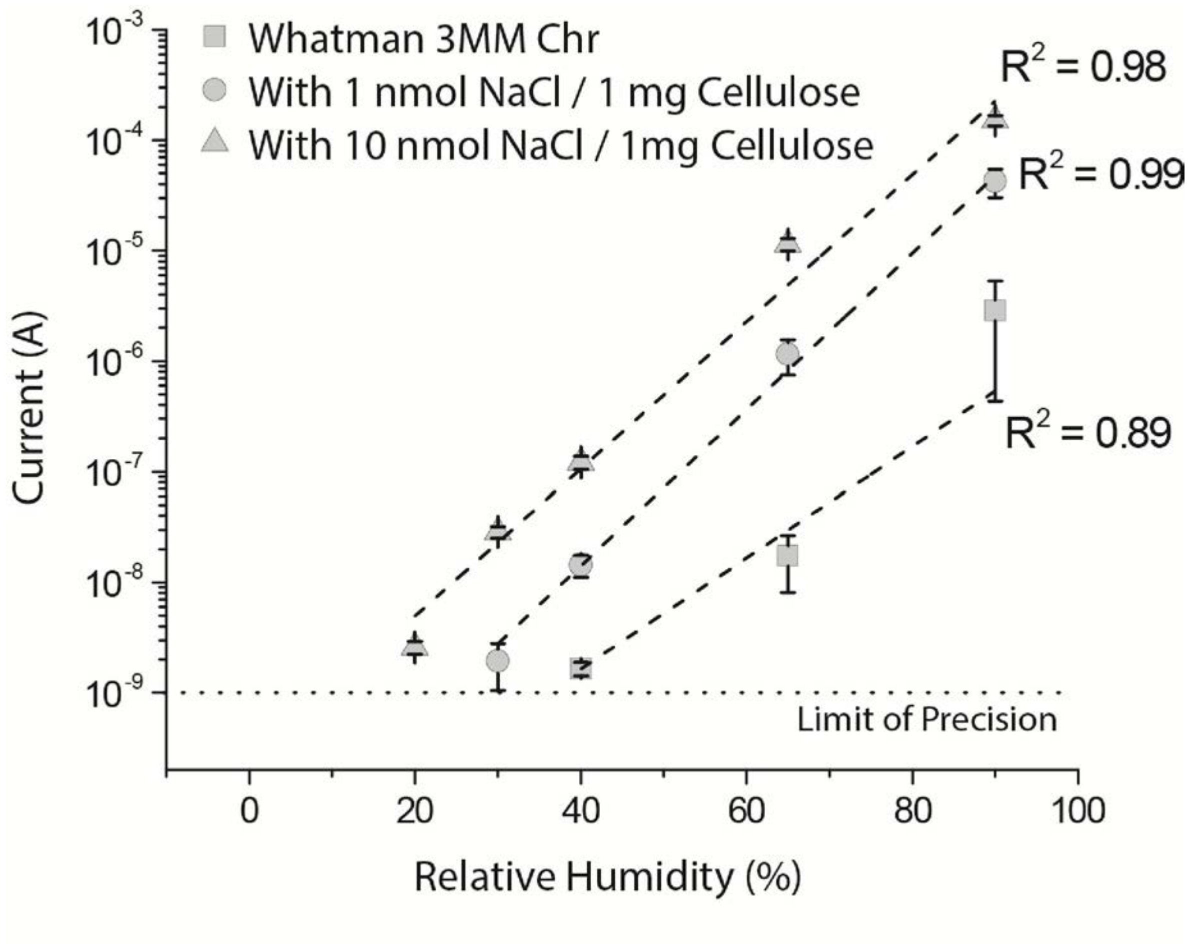

Figure S10. The effect of added NaCl on the electrical response of Whatman 3MM Chr paper at different salt concentrations. The error bars represent standard deviations (SD), N=7.

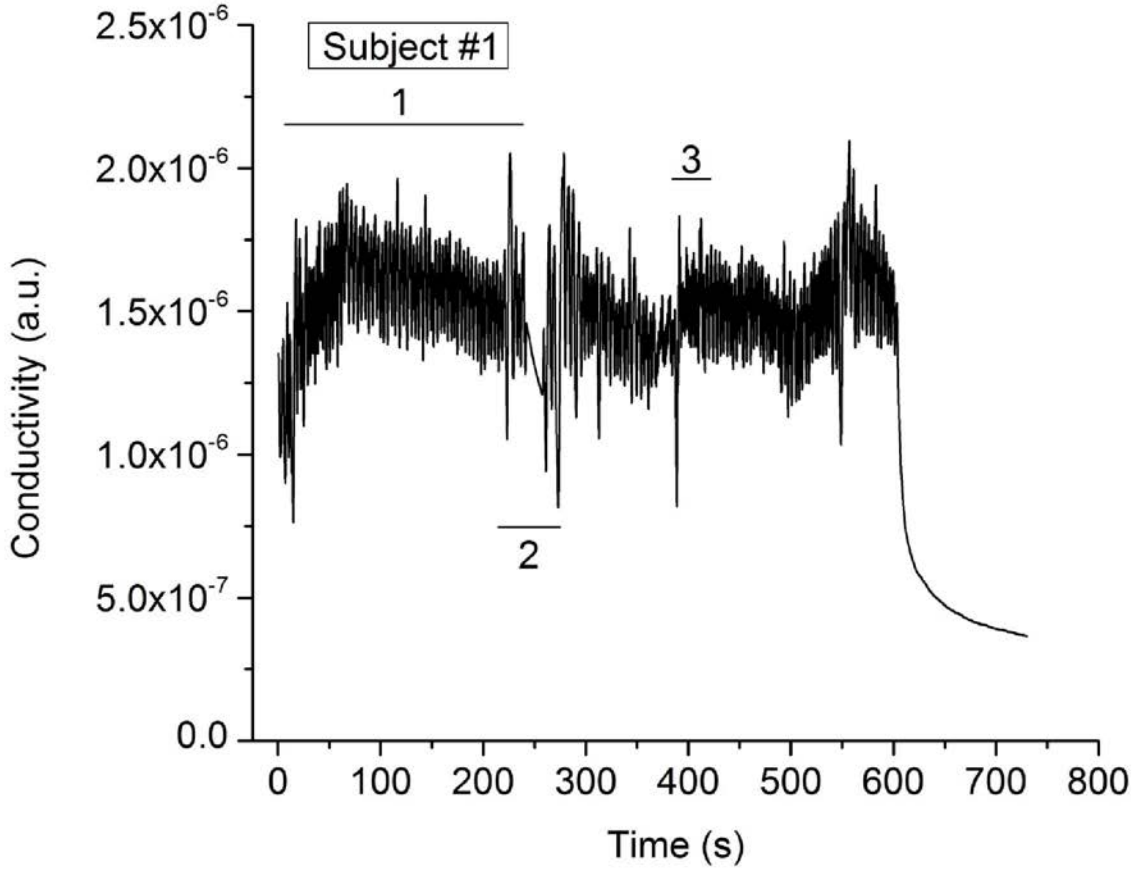

Figure S11. The resting respiratory activity of Subject #1. (1) Indicates normal, (2) paused and, (3) fast and shallow breathing

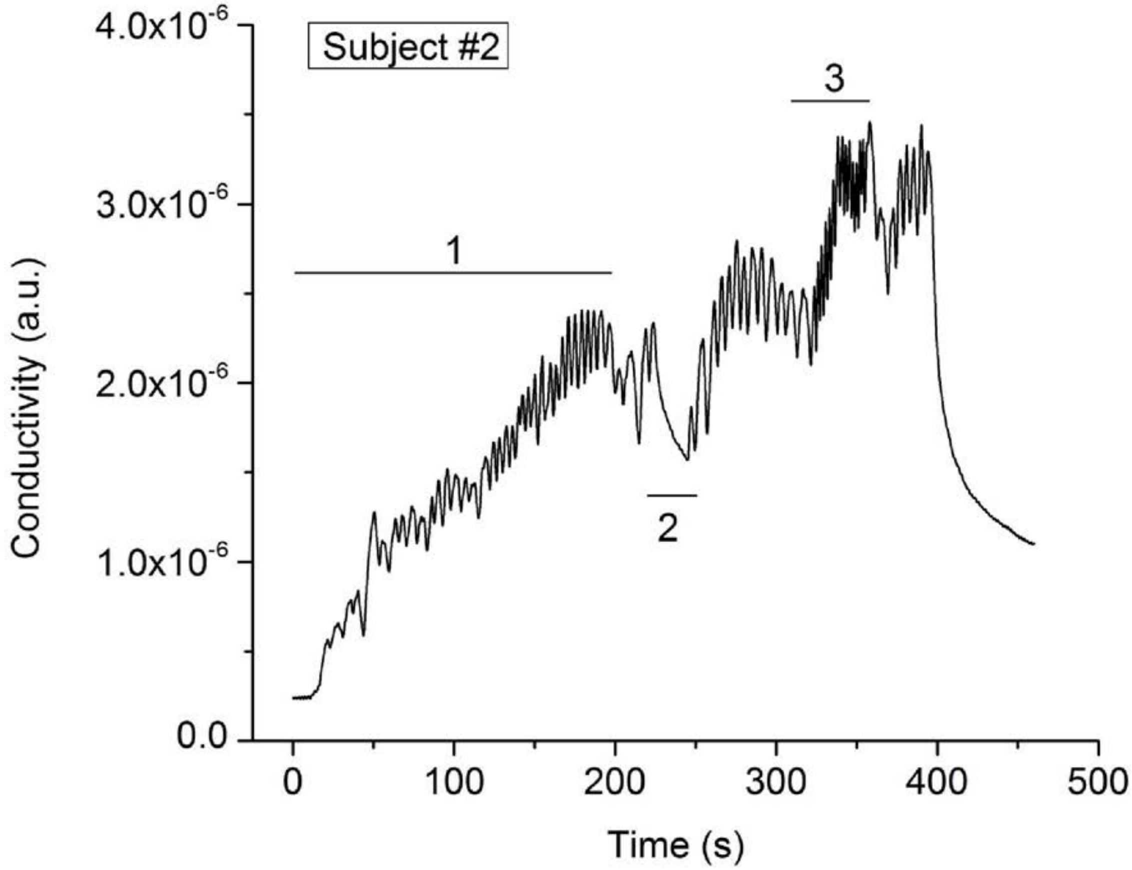

Figure S12. The resting respiratory activity of Subject #2. (1) Indicates normal, (2) paused and, (3) fast and shallow breathing

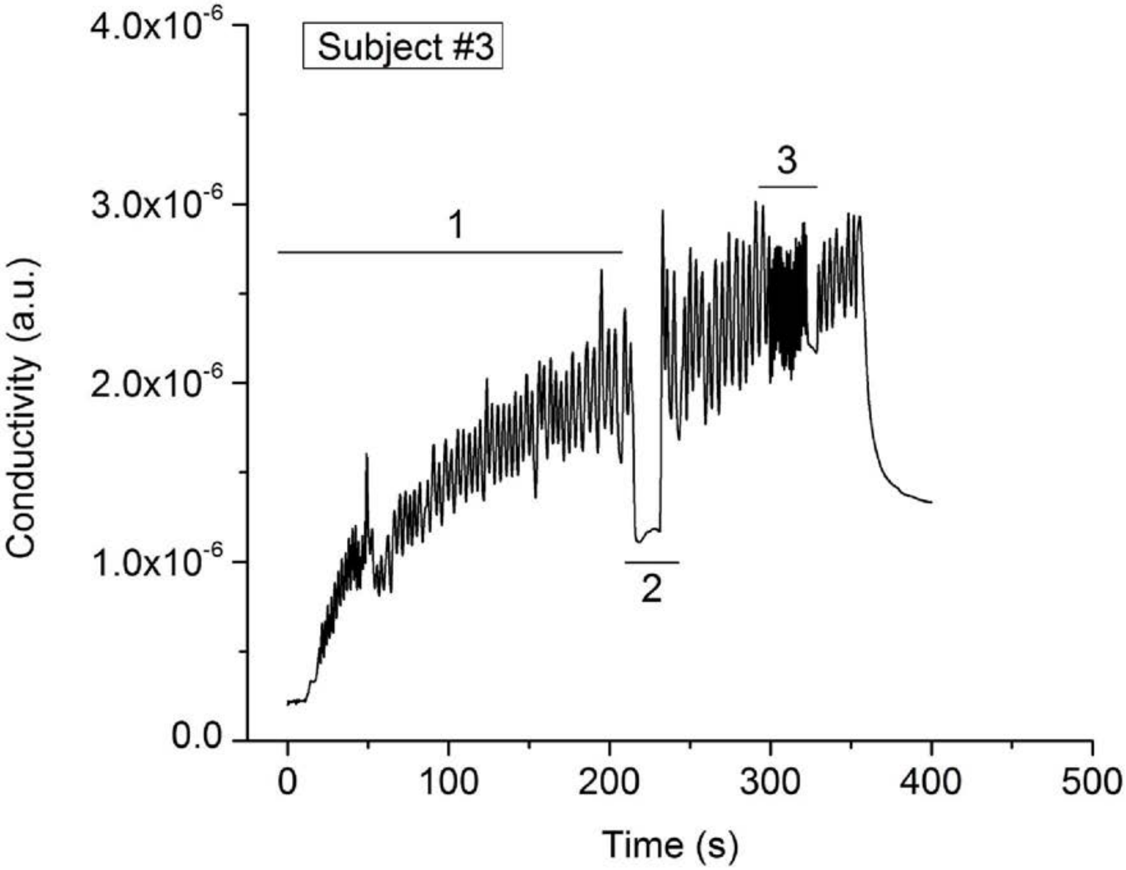

Figure S13. The resting respiratory activity of Subject #3. (1) Indicates normal, (2) paused and, (3) fast and shallow breathing

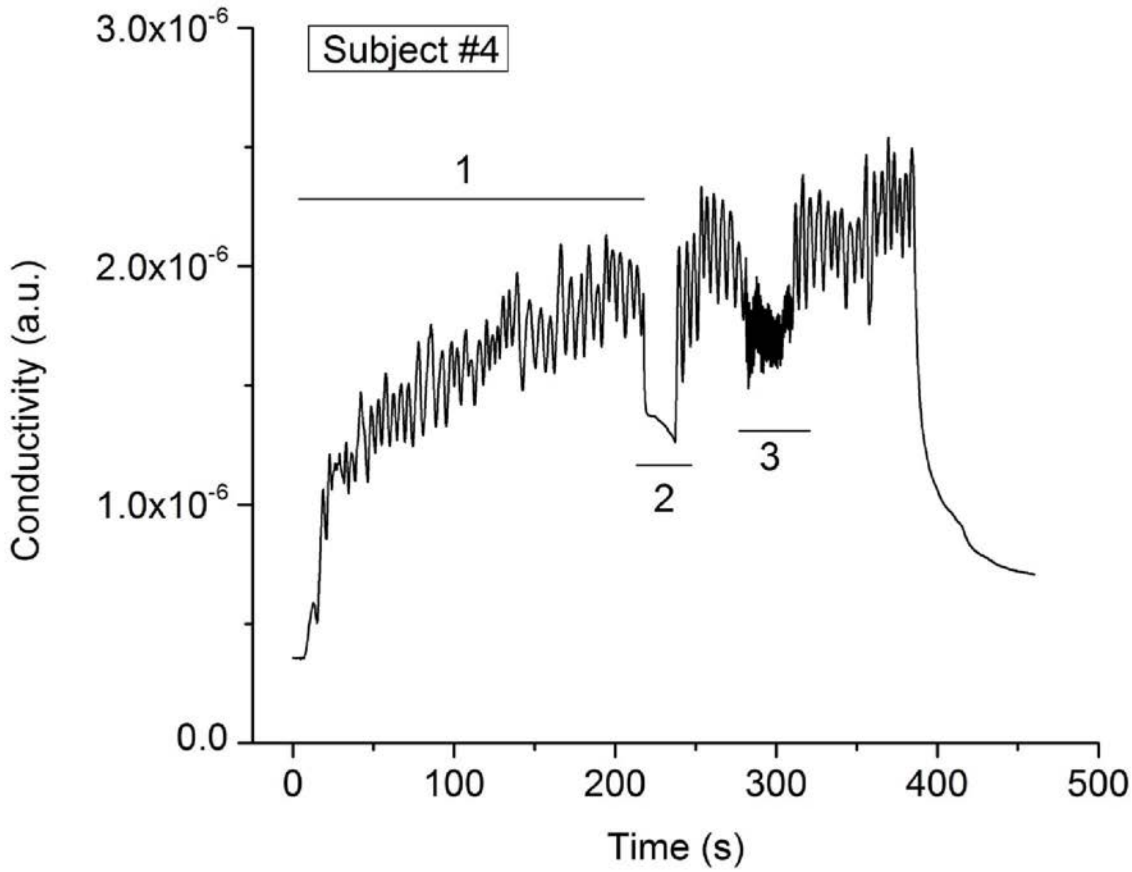

Figure S14. The resting respiratory activity of Subject #4. (1) Indicates normal, (2) paused and, (3) fast and shallow breathing

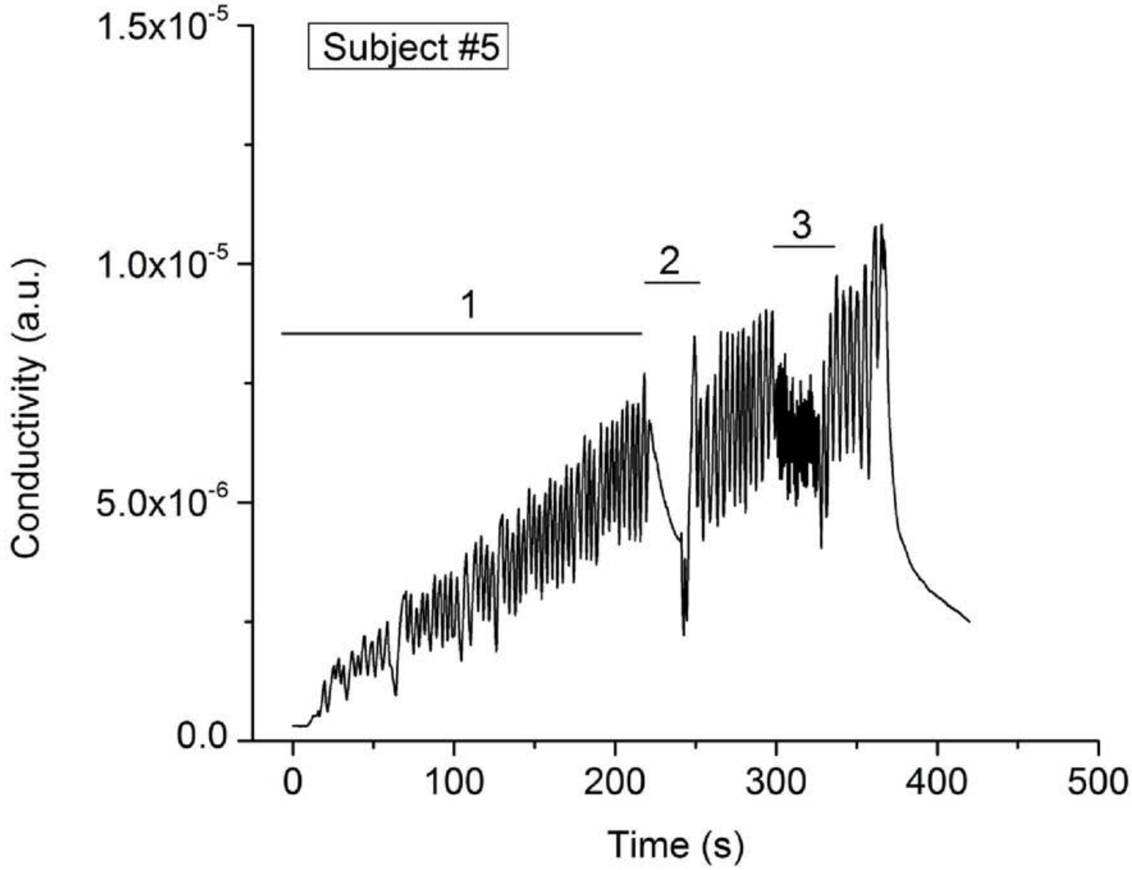

Figure S15. The resting respiratory activity of Subject #5. (1) Indicates normal, (2) paused and, (3) fast and shallow breathing

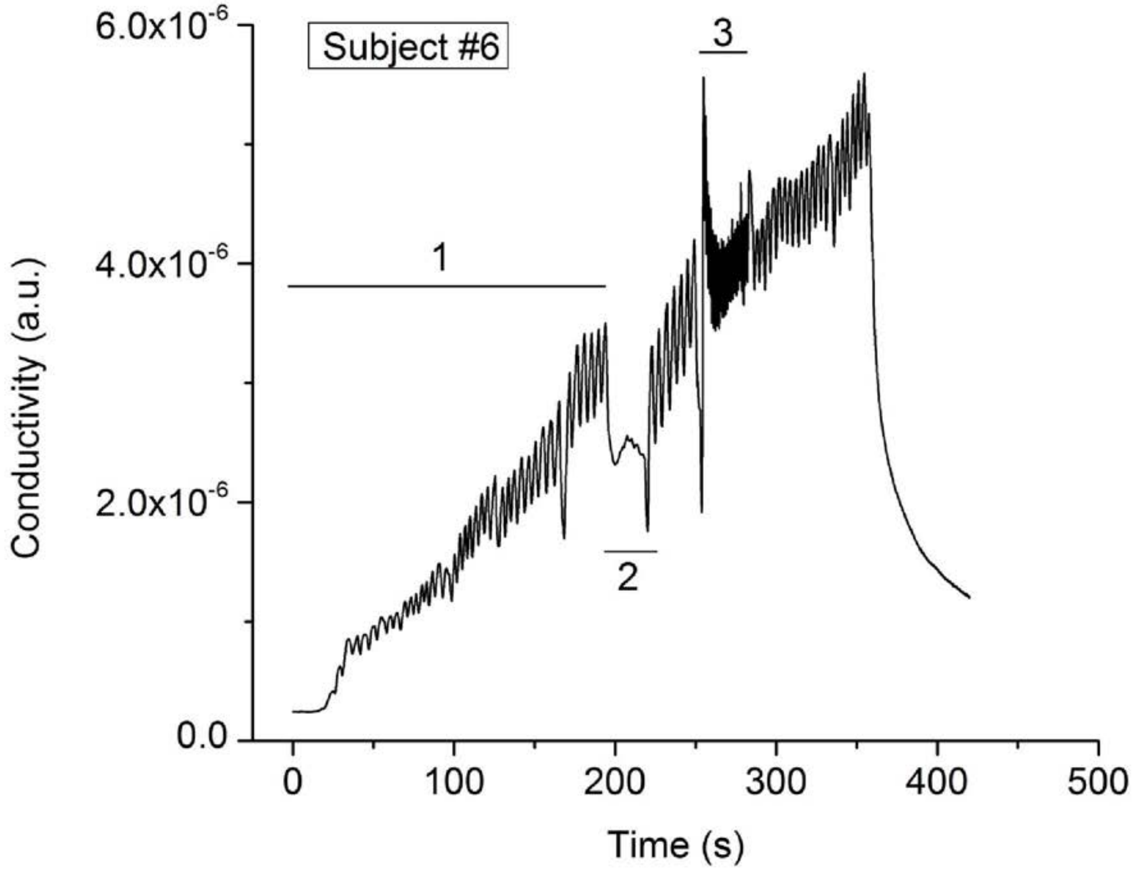

Figure S16. The resting respiratory activity of Subject #6. (1) Indicates normal, (2) paused and, (3) fast and shallow breathing

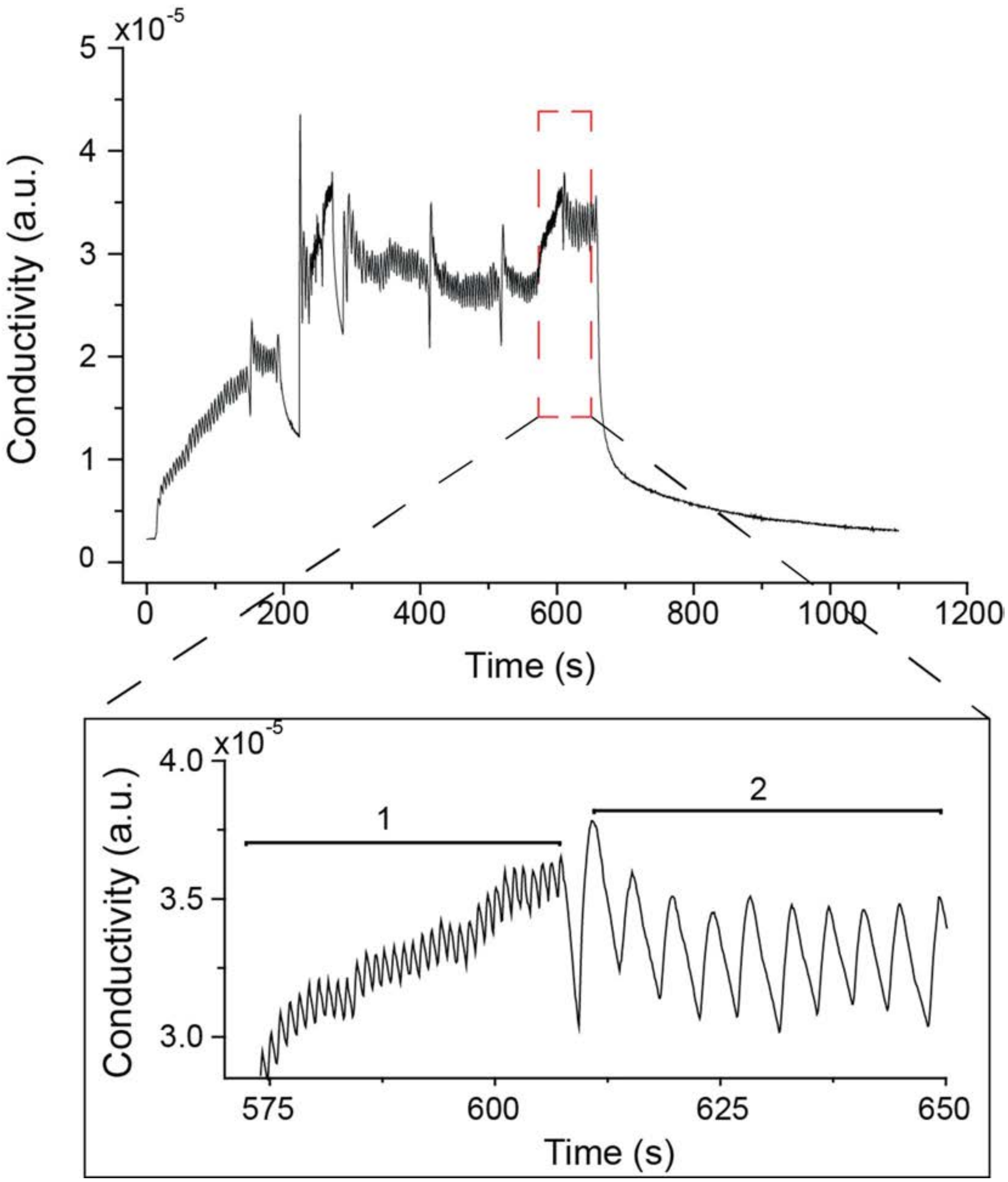

Figure S17. Plot showing the seamless transition between fast and shallow breathing (1) and normal breathing (2)

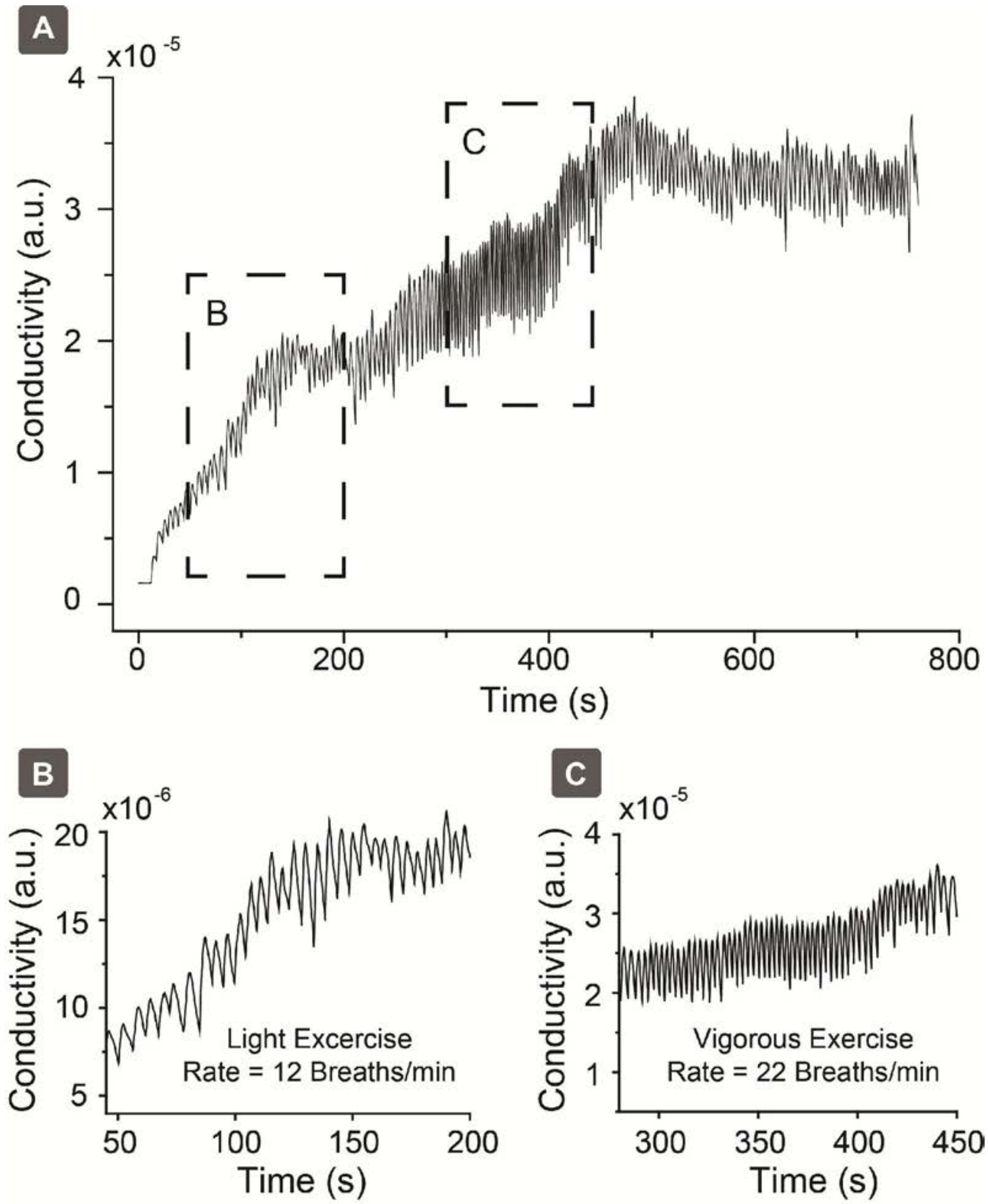

Figure S18. **(A)** Respiratory signal during light **(B)** and vigorous **(C)** exercise. The subject in this experiment had an increase in the rate of respiration from 12 breaths/min during light exercise to 22 breaths/min during vigorous exercise.

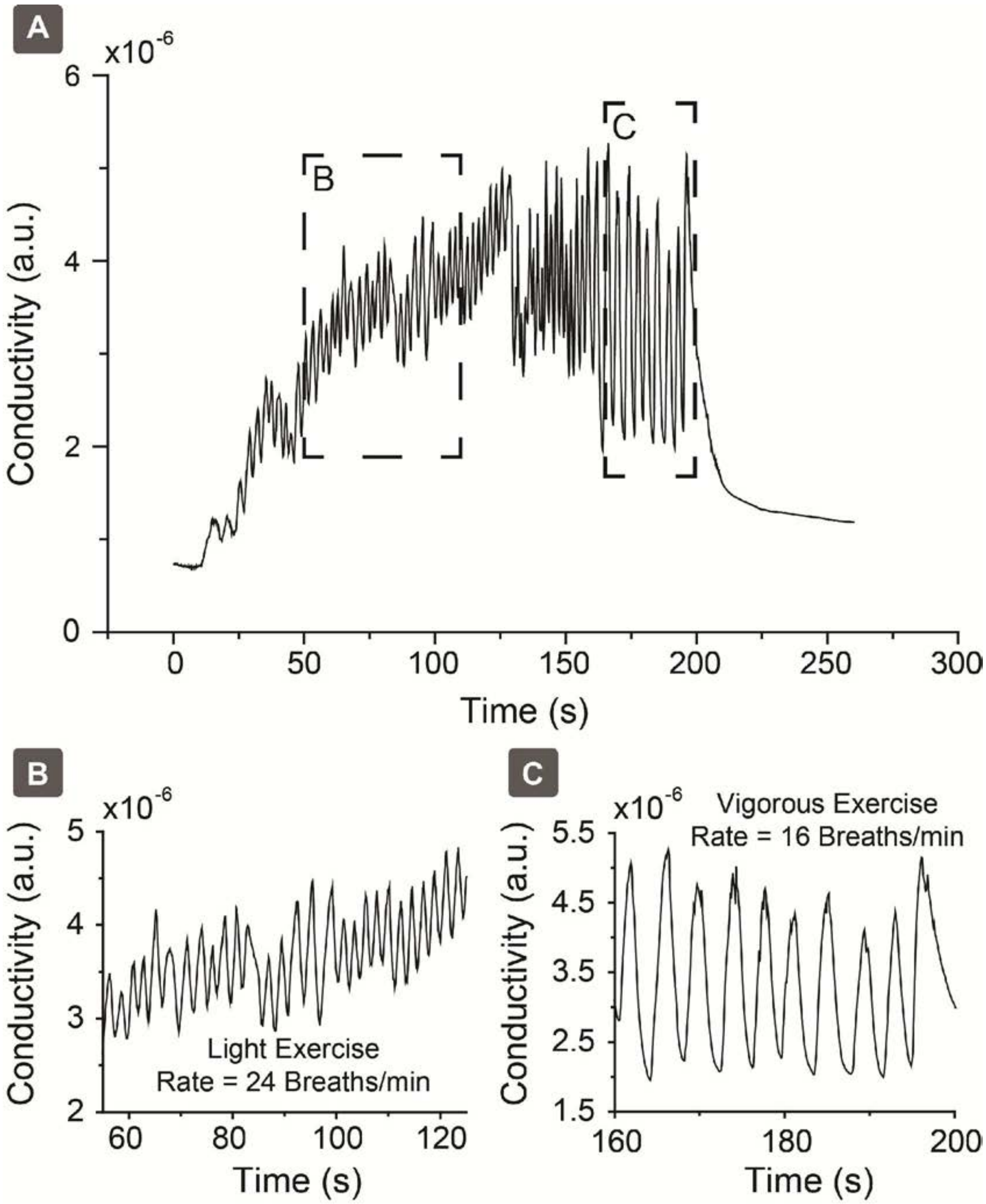

Figure S19. (A) Recorded respiratory signal during light (B) and vigorous (C) exercise. The subject in this experiment had a decrease in the rate of respiration from 24 breaths/min during light exercise to 16 breaths/min during vigorous exercise. The subject compensated for this reduction in the rate of respiration by taking deeper breaths.

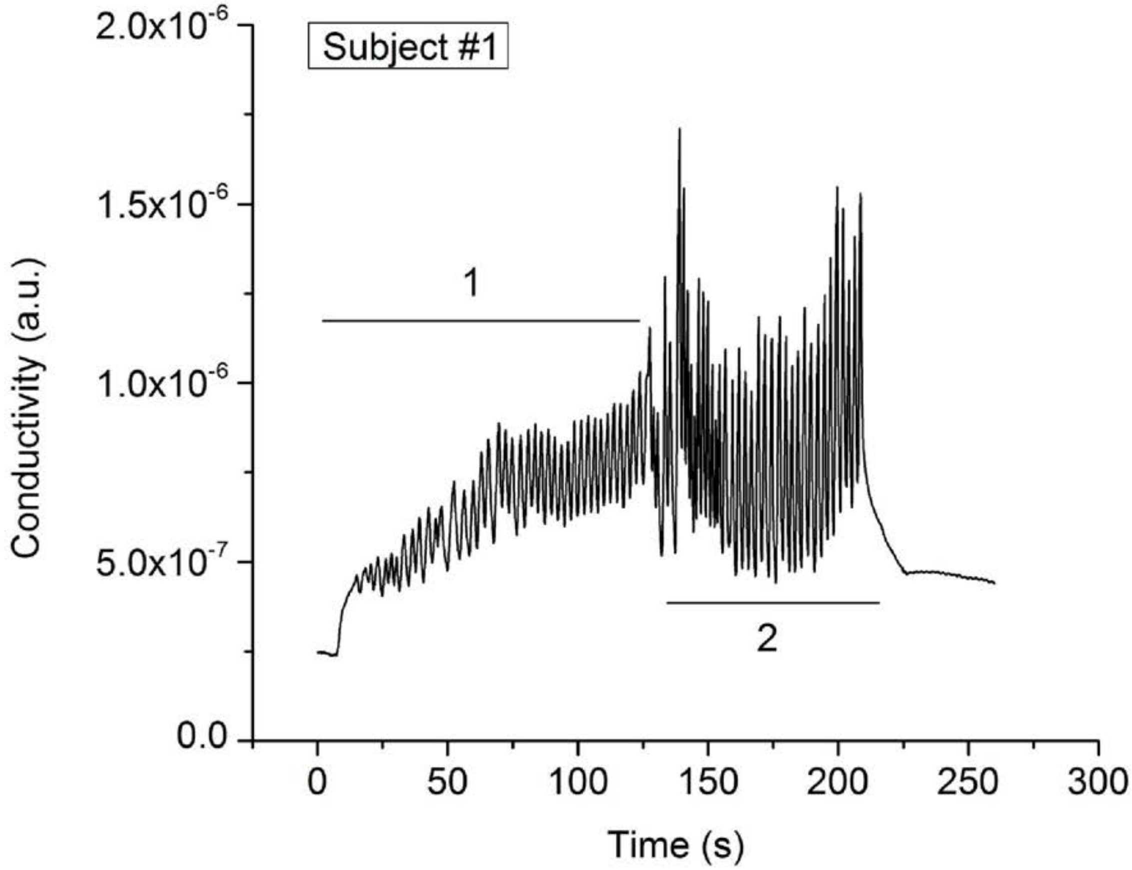

Figure S20. Recorded respiratory signal of Subject #1 during light (1) and vigorous exercise (2).

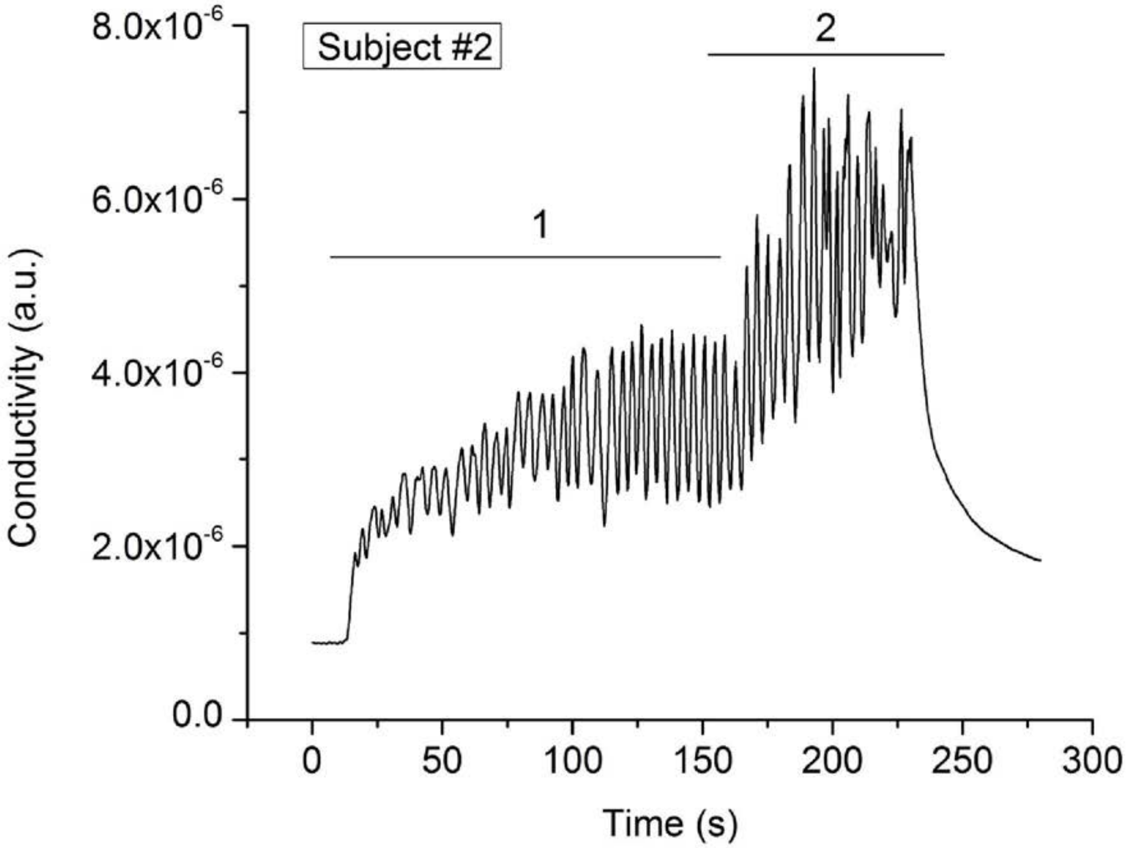

Figure S21. Recorded respiratory signal of Subject #2 during light (1) and vigorous exercise (2).

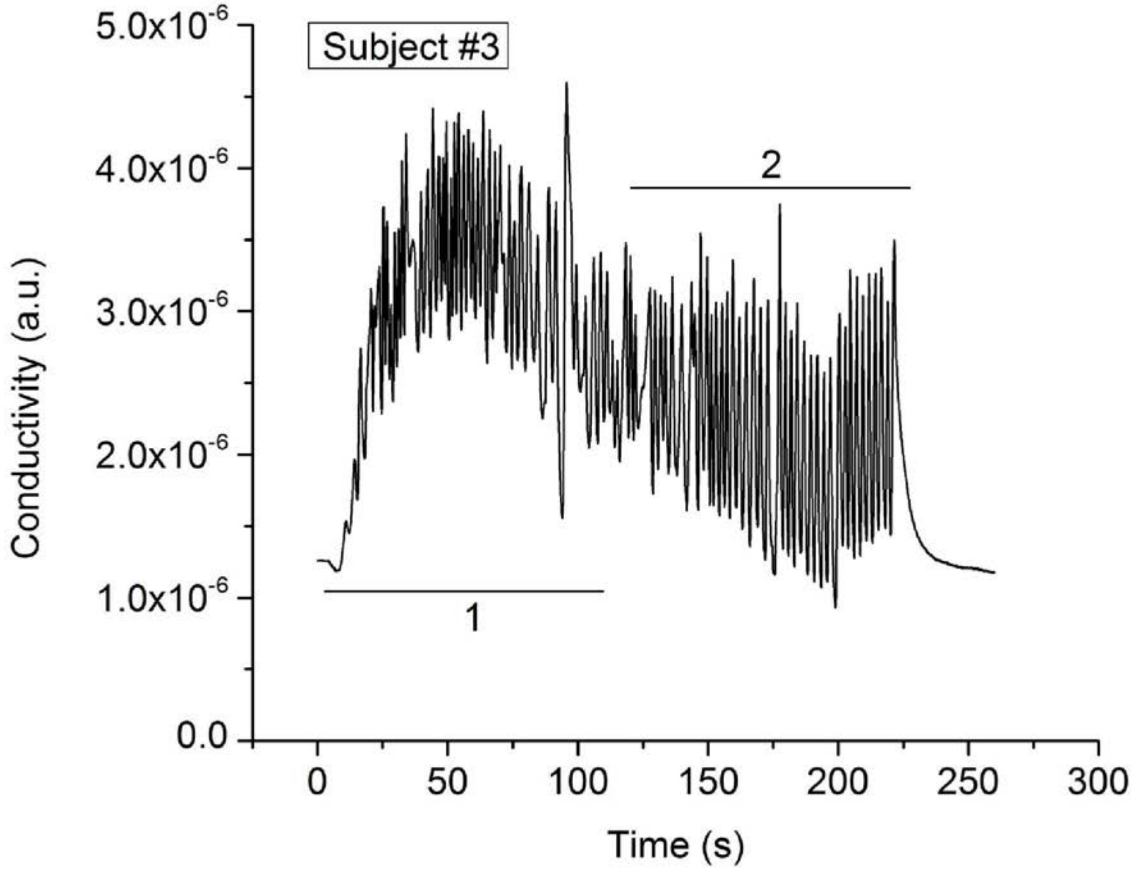

Figure S22. Recorded respiratory signal of Subject #3 during light (1) and vigorous exercise (2).

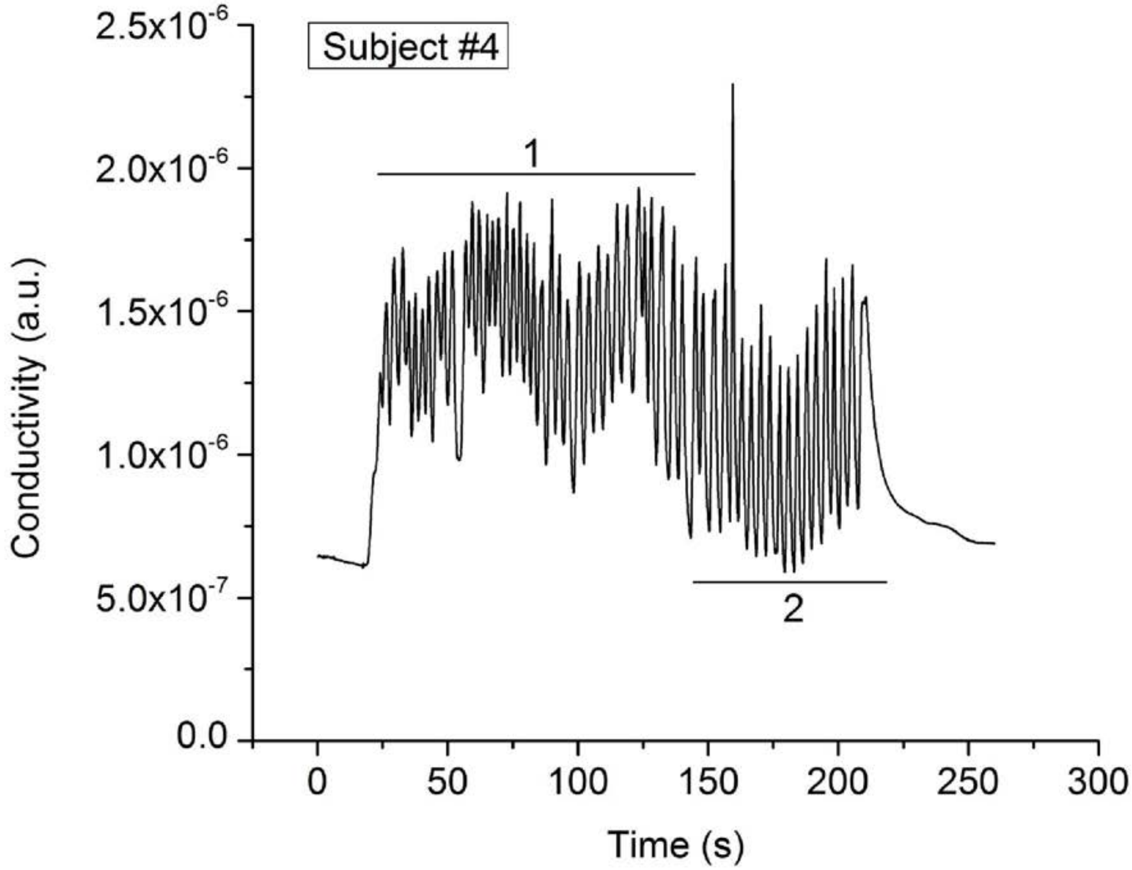

Figure S23. Recorded respiratory signal of Subject #4 during light (1) and vigorous exercise (2).

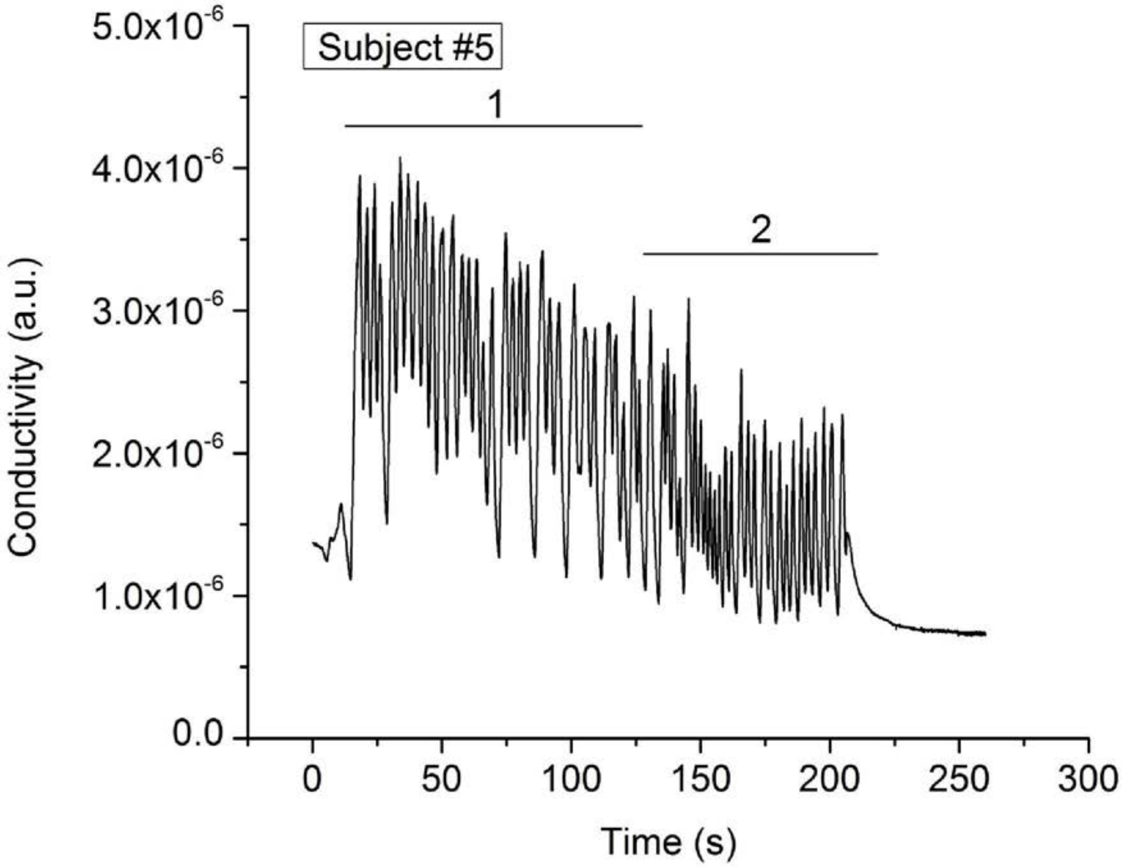

Figure S24. Recorded respiratory signal of Subject #5 during light (1) and vigorous exercise (2).

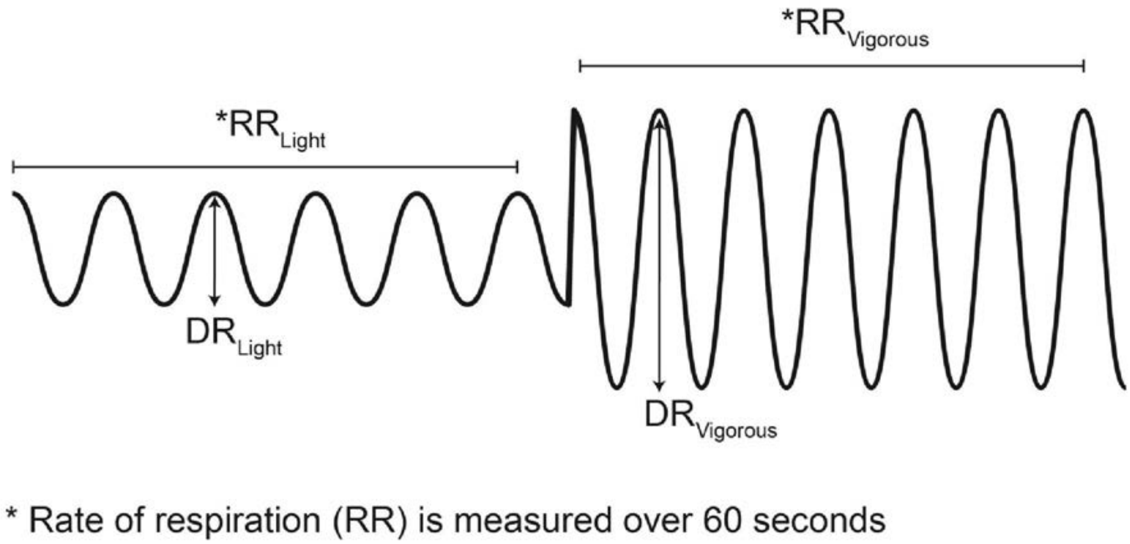

Figure S25. A conceptual waveform describing the parameters for calculating the empirical metric "Breathing Index" (BI); here, $RR_{vigorous}$ is the rate of respiration during vigorous exercise, RR_{Light} is the rate of respiration during light exercise, $DR_{Vigorous}$ is the peak-to-peak amplitude of the signal during vigorous exercise, and DR_{Light}, is the peak-to-peak amplitude of the signal during light exercise. BI is the product of the RR and DR. Since the baseline RR and DR of patients will vary between patients, we normalize the RR and DR values during vigorous exercise by the RR and DR values during light exercise for each patient, respectively.